The experiments, conducted in an 85-ft towing tank, appeared to conform the essential features of the dynamical problem as predicted by theory. A few important conclusions are summarized below: 1) The stability of a towed slender cylinder is virtually controlled by the tail portion of the cylinder which is about 25 diam from the free end. 2) For fixed value of L/D, higher modes of oscillation set in as the velocity U increases. 3) For a certain critical model, the critical velocity and frequency decrease as L/D increases. 4) As L/D increases, the minimum critical speed, frequency, and effective "wave length" that mark the threshold of instability, virtually remain at the same magnitude. 5) The lower modes of instabilities are "filtered" out and only the higher modes of instabilities set in as L/D increases. 6) For $L/D > 30$, the critical velocity and the associated frequency are $U_c[(4/_T)(c_T/E)^{1/2}] \sim 6$ and $\Omega_c[(4D/c_T^2)(\varphi/\beta E)^{1/2}] \sim 12$.

Dynamical Stability of a Towed Thin Flexible Cylinder

H. P. PAO*
The Catholic University of America, Washington, D.C.

The stability and dynamics of a slender cylinder towed in a viscous stream are examined. The cylinder is clamped at one end and free at the other. Stability conditions and modal shapes are found based on solutions to linearized equations resulting from small deflection assumptions. Particular attention is focused on the conditions of stability when the length/diameter ratio becomes large. It is found that the stability of a slender cylinder is virtually controlled by the tail portion of the cylinder which is about 25 diameters from the free end. Some experimental observations conducted in a towing tank are in general agreement with theory.

Nomenclature

c_N = $(4/\pi)C_p$
c_T = $(4/\pi)C_f$
c'_T = form drag coefficient at the tail of cylinder
C_f, C_p = frictional and pressure drag coefficients
D = diameter of cylinder
EI = flexural rigidity of cylinder
f = parameter associated with the tail end of cylinder [Eq. (7)]
F_L, F_N = longitudinal and normal viscous forces per unit length
i = apparent angle of incidence
l = length of a few cylinder diameters at the tail of cylinder
L = length of cylinder
m = mass/unit length of cylinder
M = lateral virtual mass of fluid/unit length of cylinder
Q = lateral shear force
S = cross-sectional area of cylinder
t = time
T = axial tension along cylinder
u = nondimensional fluid velocity, $(M/EI)^{1/2}\, UL$
u_c, U_c = critical velocities
U = uniform fluid velocity
$\bar{U}$ = nondimensional fluid velocity [Eq. (17)]
v = lateral velocity between the cylinder and the fluid flowing past it
x = coordinate along the center line of the undeflected cylinder
x_e = effective length of the tail of cylinder
y = lateral displacement of cylinder
β = virtual mass ratio, $M/(m + M)$
γ = $c_T \epsilon U/(4\Omega L)$
ϵ = slenderness ratio, L/D
η = nondimensional lateral displacement, y/L
ξ = nondimentional x coordinate, x/L
ρ = fluid density
ρ_b = density of cylinder
τ = nondimensional time, $[EI/(m + M)]^{1/2} t/L^2$
χ = x_e/L
ω = nondimensional circular frequency, $[(M + m)/EI]^{1/2}\Omega L^2$
ω_c, Ω_c = critical frequencies
Ω = circular frequency
$\bar{\Omega}$ = nondimensional circular frequency [Eq. (17)]

Received July 6, 1970. The author is very grateful to M. J. Casarella for his encouragement and helpful discussions during the course of this work. He is also indebted to R. H. Compton and H. Kramer for their assistance in conducting the experiments, and to U.S. Naval Academy, Hydromechanics Laboratory for permitting him to use the towing tank. This work was supported by THEMIS Program No. 893 (1968–1971) in the Institute of Ocean Science and Engineering, The Catholic University of America.

* Professor, Department of Aerospace and Atmospheric Sciences.

1. Introduction

THE purpose of this investigation is to study the free, lateral motions of submerged flexible slender cylinders held in an axial flow; the system, thus, simulates a flexible cylinder towed underwater with possible application to the submarine antennas and hydrophone array.

This work can be regarded as an extension of a previous study of the dynamics of flexible cylinders in axial flow by Paidoussis.[1,2] In his work, he studied the effect on the stability of the system for the various hydrodynamic and geometrical parameters of the system. Some of his experimental observations appeared to confirm his theoretical analysis qualitatively. However, his analysis is inadequate in so far as the effect of slenderness ratio L/D to stability is concerned, where L and D are the length and diameter of the cylinder, respectively. In this study, the effect of L/D is investigated both theoretically and experimentally. Particular attention is focused on the condition of the stability when L/D becomes large. It is found that the lower modes of instabilities are filtered out and only the higher modes of instabilities set in when L/D increases. Moreover, the minimum critical speed, frequency, and wavelength, that mark the threshold of instability, are virtually independent of L/D as the value of L/D increases. As a result, it is concluded that the stability of a slender cylinder is virtually controlled by the tail portion of the cylinder which is about 25 diameters from the free end.

In a recent paper by Ortloff and Ives,[3] the dynamic motion of a thin flexible cylinder with zero bending rigidity was studied. They found that the cylinder motion is always unstable. In this paper, some clarification and correction to the previous studies[1–3] are made toward the better understanding of the physical mechanism of the instabilities of the system.

2. General Theory

2.1 Equations of Motion of a Cylinder in a Fluid Stream

Figure 1 shows the system under consideration. It consists of a slender cylinder of circular cross section of length L, immersed in an incompressible fluid of density ρ flowing with uniform velocity U parallel to the x axis. The cylinder is considered to be clamped at the upstream end and free at the other, like a cantilever beam. The x axis coincides with the centerline of the undeflected cylinder. Apart from the tapering free end, the cylinder is of uniform cross-sectional area S, flexural rigidity EI and mass/unit length m.

The specific gravity of the cylinder is supposed to be equal to that of the flowing fluid. The x and y axis lie in a horizontal plane wherein all motions of the cylinder are supposed to be confined, so that gravity and buoyancy do not come into play.

Following Paidoussis[1] and Gregory and Paidoussis,[4] the equations governing the motion of a flexible cylinder immersed in a uniform stream are

$$(\partial T/\partial x) + F_L = 0 \tag{1}$$

$$EI(\partial^4 y/\partial x^4) + F_N - (\partial/\partial x)(T\,\partial y/\partial x) + M[(\partial/\partial t) + U(\partial/\partial x)]^2 y + m(\partial^2 y/\partial x^2) = 0 \tag{2}$$

where T is the axial tension and M is the lateral virtual mass of fluid/unit length of cylinder. Equations (1) and (2) represent the balance of forces in the longitudinal and normal directions on an element of cylinder (Fig. 2). The terms F_L and F_N represent the viscous forces/unit length in the longitudinal and normal directions, respectively. Further assumptions regarding the derivation of (1) and (2) are listed in Ref. 1.

The viscous forces acting on long inclined cylinders have been discussed by Reber,[5] Hoerner,[6,7] Taylor,[8] and many others. A comprehensive survey on the hydrodynamic loading on cable systems was recently given by Parsons and Casarella.[9] For turbulent boundary layers, the viscous forces are

$$F_N = \tfrac{1}{2}\rho D U^2(C_p \sin^2 i + C_f \sin i),\ F_L = \tfrac{1}{2}\rho D U^2 C_f \cos i \tag{3}$$

where C_p and C_f are the coefficients associated with pressure and frictional drag for a cylinder in cross flow and i is the apparent angle of incidence which may be related by

$$i = \sin^{-1}(v/U) = \sin^{-1}\{[(\partial y/\partial t) + (U\partial y/\partial x)]/U\}$$

where v is the lateral velocity between the cylinder and the fluid flowing past it. For small motions of the cylinder, i is small so that Eq. (3) becomes

$$F_N \simeq \frac{1}{2}\frac{M}{D} U c_N \left(\frac{\partial y}{\partial t} + U\frac{\partial y}{\partial x}\right),\ F_L \simeq \frac{1}{2}\frac{M}{D} U^2 c_T \tag{4}$$

in which ρ was eliminated by $\rho = 4M/\pi D^2$; terms of the order of i^2 have been neglected; $c_N = (4/\pi)C_p$ and $c_T = (4/\pi)C_f$. From Eqs. (1) and (4), the axial tension is

$$T(x) = T(L) + \tfrac{1}{2}(M/D)U^2 c_T(L - x)$$

A nonzero value of $T(L)$ can only arise from form drag at the free end, which may be considered proportional to $\frac{1}{2}\rho U^2 S$.

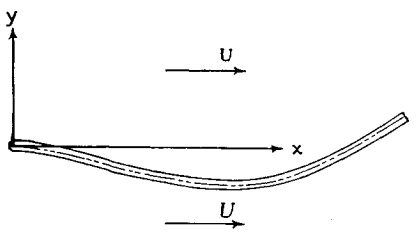

Fig. 1 Schematic diagram of the system.

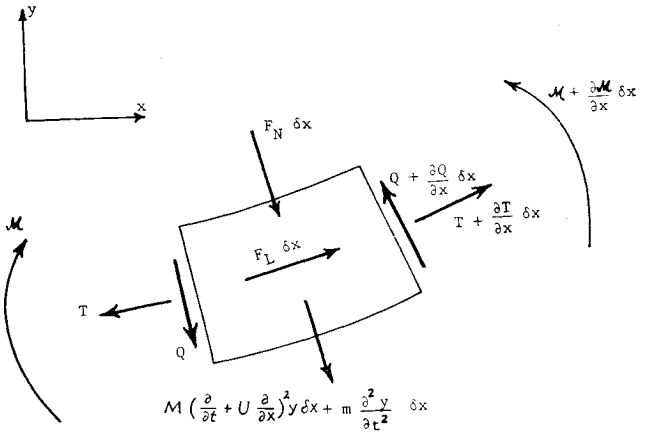

Fig. 2 Forces and moments acting on an element δx of the cylinder.

Accordingly, we write

$$T(x) = \tfrac{1}{2}c'_T M U^2 + \tfrac{1}{2}(M/D)U^2 c_T(L - x) \tag{5}$$

where c'_T is the coefficient of form drag at the tail.

Substituting now Eqs. (3–5) into Eq. (2), we obtain the equation of small lateral motions,

$$EI\frac{\partial^4 y}{\partial x^4} + M\left(\frac{\partial}{\partial t} + U\frac{\partial}{\partial x}\right)^2 y - \frac{\partial}{\partial x}\left[\left(\frac{1}{2}c_T\frac{L - x}{D} + \frac{1}{2}c'_T\right)MU^2\frac{\partial y}{\partial x}\right] + \frac{1}{2}c_N\frac{MU}{D}\left(\frac{\partial y}{\partial t} + U\frac{\partial y}{\partial x}\right) + m\frac{\partial^2 y}{\partial t^2} = 0 \tag{6}$$

It is noted that Eq. (6) is not quite valid near the downstream free end because of 1) the lateral flow not being truly two-dimensional, since the fluid can pass around, rather than over the free end (see Ref. 10) and 2) nonuniform cross-sectional area S because of the tapering at the free end. Therefore, Eq. (6) is to be applied for $0 \leqslant x \leqslant L - l$ where l is at most a few cylinder diameters. For $L - l < x \leqslant L$, a separate equation must be derived.

2.2 Boundary Conditions

When the upstream end is clamped, the boundary conditions are $y = \partial y/\partial x = 0$ at $x = 0$. At the downstream free end, it is assumed that the cross-sectional area tapers smoothly from S to zero in a distance sufficiently short, so that the lateral velocity v may be considered constant. This requirement allows the forces acting at the free end to be lumped and considered in appropriate boundary conditions similar to those given by Hawthorne[11] and Paidoussis.[1] It should be noted that even if there is no tapering at the free end, the following derivation is still valid. Integrating a similar equation like Eq. (6) from $x = L - l$ to $x = L$, we obtain

$$-\int_{L-l}^{L}\frac{\partial Q}{\partial x}\,dx + f\int_{L-l}^{L}\left(\frac{\partial}{\partial t} + U\frac{\partial}{dx}\right)[M(x)v]\,dx + \int_{L-l}^{L}F_N\,dx - \int_{L-l}^{L}\frac{\partial}{\partial x}\left(T\frac{\partial y}{\partial x}\right)dx + \int_{L-l}^{L}m(x)\frac{\partial^2 y}{\partial t^2}\times dx = 0 \tag{7}$$

where Q is the lateral shear force. The parameter f, which is equal to unity for slender body, inviscid flow theory, was introduced to account for the theoretical lateral force at the free end not being fully realized because of 1) the lateral flow not being truly two dimensional and 2) boundary-layer effects.[10] Accordingly, f will normally be less than unity. In our experimental investigation, the free end of the cylinder was left blunt and no tapered end pieces were used. A value of 0.7 was chosen for f that appeared to agree with theory qualitatively.

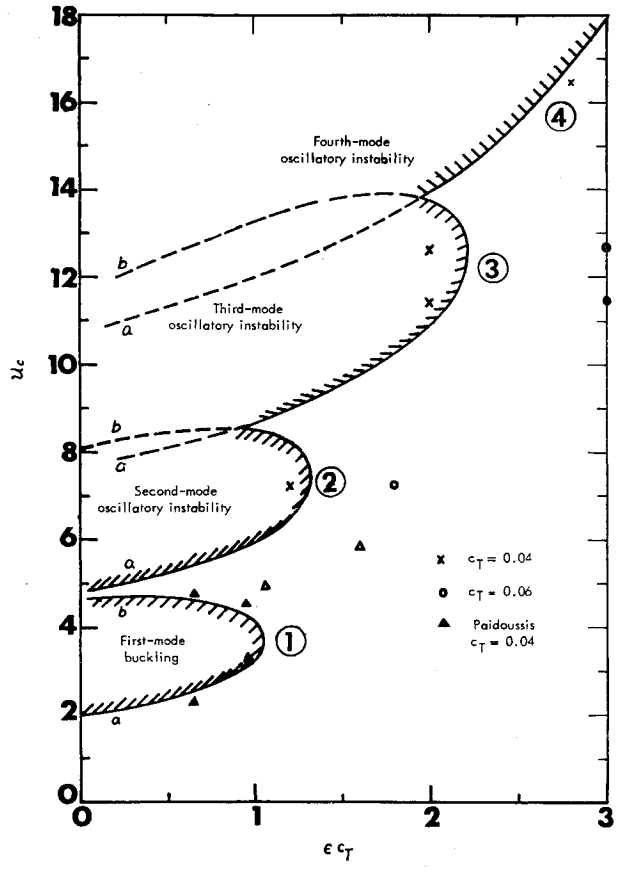

Fig. 3a) Stability map showing the effect of the slenderness ratio ϵ on the stability of clamped-free cylinders (β = 0.5, χ = 0.01, f = 0.7, c'_T = 0.2, $c_N = c_T$).

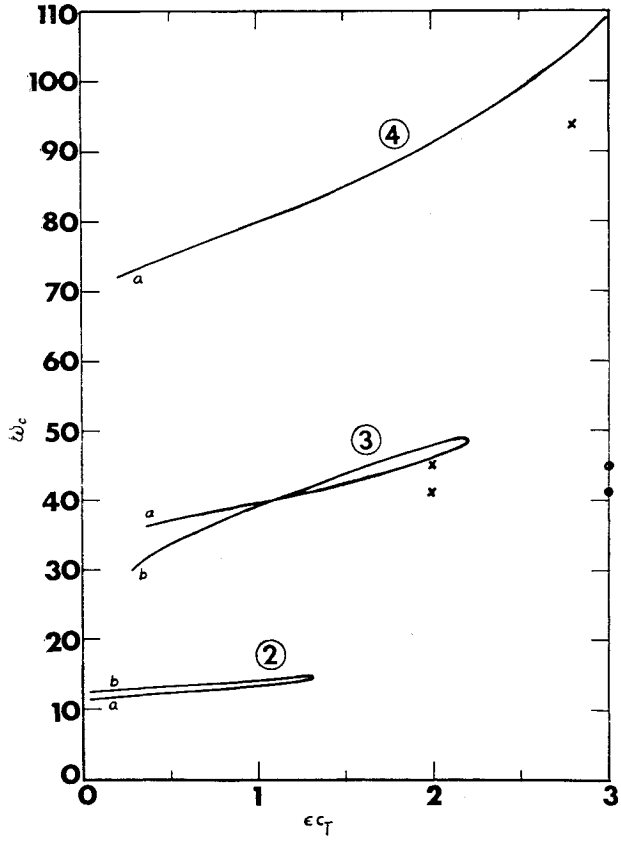

Fig. 3b) Corresponding frequency associated with the neutral stability.

We now write $M(x) = \rho S(x)$ and $m(x) = \rho_b S(x)$ and, since v is considered constant for $L - l < x < L$ (provided that $l/L \ll 1$) and Q is zero at the free end, Eq. (7) leads to

$$\left[EI\frac{\partial^3 y}{\partial x^3} + fMU\left(\frac{\partial y}{\partial t} + U\frac{\partial y}{\partial x}\right) - (m + fM)x_e\frac{\partial^2 y}{\partial t^2}\right]_{x=L-l} - \frac{1}{2}c_N\left(\frac{M}{D}\right)U\frac{\partial y}{\partial t}\,l - \left[\frac{1}{2}c_N\left(\frac{M}{D}\right)U^2 y - T\frac{\partial y}{\partial x}\right]\Bigg|_{x=L-l}^{x=L} = 0 \tag{8}$$

where

$$x_e = \frac{1}{S}\int_{L-l}^{L} S(x)dx$$

If Eq. (8) is written in dimensionless form, some terms are of order l/L or smaller. Hence, on neglecting terms of small magnitude, we obtain

$$EI\frac{\partial^3 y}{\partial x^3} + fMU\left(\frac{\partial y}{\partial t} + U\frac{\partial y}{\partial x}\right) - (m + fM)\,x_e\frac{\partial^2 y}{\partial t^2} = 0 \quad \text{at } x = L - l \tag{9}$$

in which the third term involving x_e could have been neglected. It is, however, kept here in order to compare the present computations with those given by Paidoussis.[1,2]

A second boundary condition at the free end can similarly be derived by integrating the dynamic equation with respect to x twice from $x = L - l$ to $x = L$. Assuming that there is no bending moment at the free end and neglecting terms of order l/L or smaller, we obtain

$$\partial^2 y/\partial x^2 = 0 \text{ at } x = L - l \tag{10}$$

These are similar to the boundary conditions derived by Hawthorne[11] and Paidoussis.[1] It is understood that $l/L \ll 1$ so that the boundary conditions (9) and (10) may be considered to apply at $x = L$.

2.3 Analysis

The problem is expressed in dimensionless terms by putting

$$\xi = \frac{x}{L},\ \eta = \frac{y}{L},\ \tau = \left(\frac{EI}{m+M}\right)^{1/2}\frac{t}{L^2},\ \beta = \frac{M}{m+M} \tag{11}$$

$$\epsilon = \frac{L}{D},\ \chi = \frac{x_e}{L},\ u = \left(\frac{M}{EI}\right)^{1/2}UL,\ \omega = \left(\frac{M+m}{EI}\right)^{1/2}\Omega L^2$$

Substituting into Eq. (6), we obtain

$$\frac{\partial^4\eta}{\partial\xi^4} + u^2\left[1 - \frac{1}{2}\epsilon c_T(1-\xi) - \frac{1}{2}c'_T\right]\frac{\partial^2\eta}{\partial\xi^2} + 2\beta^{1/2}u\frac{\partial^2\eta}{\partial\xi\partial\tau} + \frac{1}{2}\epsilon(c_N + c_T)\,u^2\frac{\partial\eta}{\partial\xi} + \frac{1}{2}\epsilon c_N\beta^{1/2}u\frac{\partial\eta}{\partial\tau} + \frac{\partial^2\eta}{\partial\tau^2} = 0 \tag{12}$$

Similarly, the boundary conditions are

$$\eta = \frac{\partial\eta}{\partial\xi} = 0 \text{ at } \xi = 0$$

$$\frac{\partial^2\eta}{\partial\xi^2} = \frac{\partial^3\eta}{\partial\xi^3} + fu^2\frac{\partial\eta}{\partial\xi} + f\beta^{1/2}u\frac{\partial\eta}{\partial\tau} - [1 + (f-1)\beta]\chi\times \frac{\partial^2\eta}{\partial\tau^2} = 0 \text{ at } \xi = 1 \tag{13}$$

It is noted that β may in principle vary from 0 to 1; the lower limit corresponds to a very light fluid and a very heavy cylinder, and the higher limit to the opposite case. However, the assumption of null buoyancy made earlier (Sec. 2) necessitates that $\beta = \frac{1}{2}$.

Let us now consider motions of the cylinder of the form

$$\eta = Y(\xi)e^{i\omega\tau} \tag{14}$$

ω being a dimensionless frequency defined in Eq. (11), where Ω is the circular frequency of motion which in general is complex. The system will be stable or unstable accordingly as the imaginary part of ω is positive or negative. Substituting Eq. (14) into Eqs. (12) and (13), we obtain

$$\frac{d^4Y}{d\xi^4} + a\frac{d^2Y}{d\xi^2} + b\xi\frac{d^2Y}{d\xi^2} + c\frac{dY}{d\xi} + eY = 0 \tag{15}$$

$$Y(0) = \left(\frac{dY}{d\xi}\right)_{\xi=0} = 0 \tag{16}$$

$$\left(\frac{d^2Y}{d\xi^2}\right)_{\xi=1} = \left(\frac{d^3Y}{d\xi^3} + h\frac{dY}{d\xi} + jY\right)_{\xi=1} = 0$$

where

$$a = u^2(1 - \tfrac{1}{2}\epsilon c_T - \tfrac{1}{2}c'_T),\ b = \tfrac{1}{2}\epsilon c_T u^2,$$

$$c = \tfrac{1}{2}\epsilon(c_N + c_T)u^2 + 2\beta^{1/2}u\omega i,\ e = -\omega^2 + \tfrac{1}{2}\epsilon c_N\beta^{1/2}u\omega i,$$

$$h = fu^2, \text{ and } j = f\beta^{1/2}u\omega i + [1 + (f-1)\beta]\chi w^2$$

The method of analysis is to express $Y(\xi)$ as a power series in ξ, so that

$$Y(\xi) = \sum_{r=0}^{\infty} A_r\xi^r$$

where the A_r are generally complex. Substituting this series into Eqs. (15) and (16), we eventually obtain 2×2 determinant which must vanish for nontrivial solution[1]; this provides an implicit relation between ω and u for any prescribed physical parameters of the system.

3. Conditions of Stability

For any given physical system, we suppose that the system parameters can be calculated or measured, and that they are independent of the flow velocity. The conditions of stability have been investigated by calculating systematically the critical flow velocities for neutral stability and their associated frequencies. The results are shown in Fig. 3. For a given set of system parameters and for each mode, the values of u and $Re(\omega)$ were determined by the method given in Sec. 3, with the condition that $Im(\omega) = 0$. To start the computation, however, the complex frequency of each mode is calculated for $\epsilon c_{NT} = 1$, starting with $u = 0$ and increasing the flow velocity in small steps, as shown in Fig. 4. The results demonstrate the general character of the dynamic behavior of the system for varying u. The critical flow velocity u_c for neutral stability and corresponding frequency which will be denoted by ω_c then are obtained from Fig. 4 by setting $Im(\omega) = 0$. Now, varying ϵc_T in either directions systematically with $Im(\omega) = 0$, we obtain the stability map as shown in Fig. 3. The computations are also aided and checked by calculating the complex frequency for some other values of ϵc_T, such as the one displayed in Fig. 5. For $\epsilon c_T = 2.5$, it is seen that the system is stable with respect to the first three modes, it is, nevertheless, unstable with respect to the fourth and higher modes.

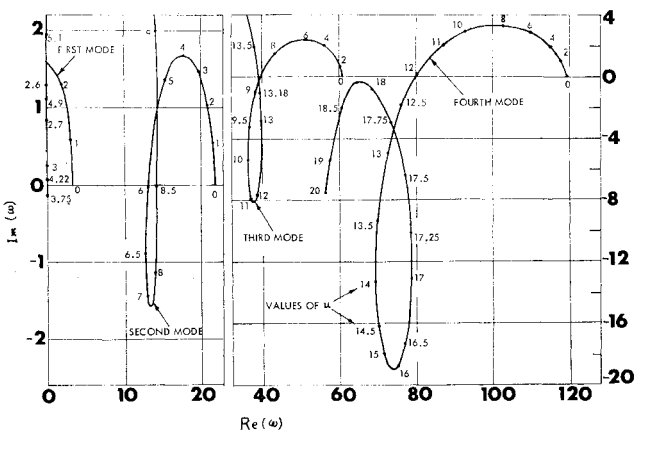

Fig. 4 The dimensionless complex frequency of first four modes of a system with $\epsilon c_T = \epsilon c_N = 1.0$, $\beta = 0.5$, $c'_T = 0.2$, $f = 0.7$, $\chi = 0.01$.

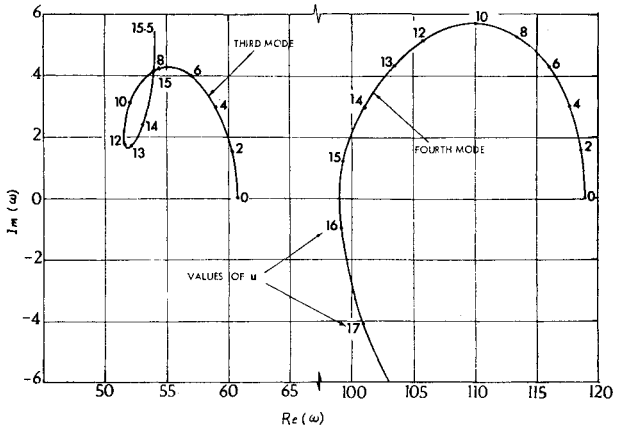

Fig. 5 The dimensionless complex frequency of the third and fourth modes of a system with $\epsilon c_T = \epsilon c_N = 2.5$, $\beta = 0.5$, $c'_T = 0.2$, $f = 0.7$, $\chi = 0.01$.

It is interesting to note that each mode has two branches, one higher and the other lower, according to the critical flow velocities.† Likewise, the corresponding frequencies has also two branches for each mode as shown in Fig. 3b. Nevertheless the frequencies differ very little between the two branches of the same mode. For a given value of ϵc_T, the system is stable for small values of u. As the flow velocity increases, however, the system may become unstable. For $\epsilon c_T < 1.05$, the system first becomes unstable to a lower buckling mode 1a as shown in Fig. 3a. Transition from lower buckling to higher buckling mode occurs as u increases. At higher-flow velocities, the system then spontaneously develops second-mode unstable oscillation which shifts from the mode corresponding to the lower branch to the higher branch.

At still higher flow velocities, third-mode and then higher-mode unstable oscillations will develop. The previous general behavior of the system for increasing flow velocity is in substantial agreement with the experimental observations by Paidoussis[2] and this author. For $\epsilon c_T > 1.05$, the buckling-mode instability cannot occur. In other words, the buckling-mode instability is filtered out of the system. As the value of ϵc_T becomes larger, more lower modes are filtered out. The physical reasoning appears to be that as ϵc_T increases the longitudinal tension along the cylinder also increases due to the frictional drag, and as a consequence lower modes of instability are suppressed.

In Fig. 3, at $\epsilon c_T \sim 1.25$, the system is unstable to second-mode oscillation for $7.0 < u < 8.0$. Transition from lower branch to higher branch of the instability mode is probably the explanation of the phenomenon observed by Paidoussis.[2] He stated "When $\epsilon > 40$ there was no second-mode instability. At $\epsilon = 39.6$ the amplitude and frequency of oscillation were erratic, ..."

It is also seen in Fig. 3 that both u_c and ω_c become larger for higher modes. A large number of terms in the power

† The lower branches of the first and second modes were first calculated by Paidoussis.[1]

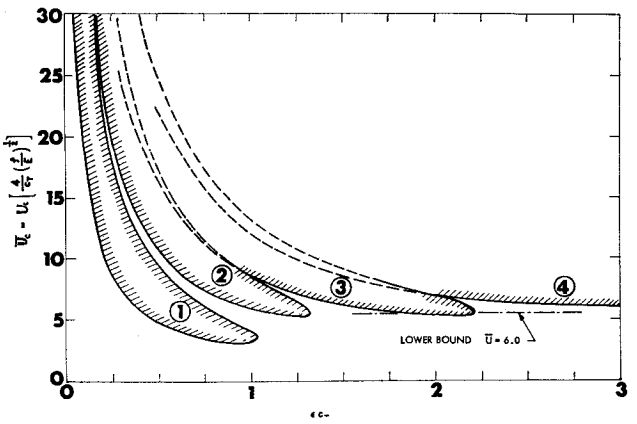

Fig. 6a) The dimensionless critical flow velocity $\bar{U}_c$ as a function of ϵc_T ($\beta = 0.5$, $\chi = 0.01$, $f = 0.7$, $c'_T = 0.2$).

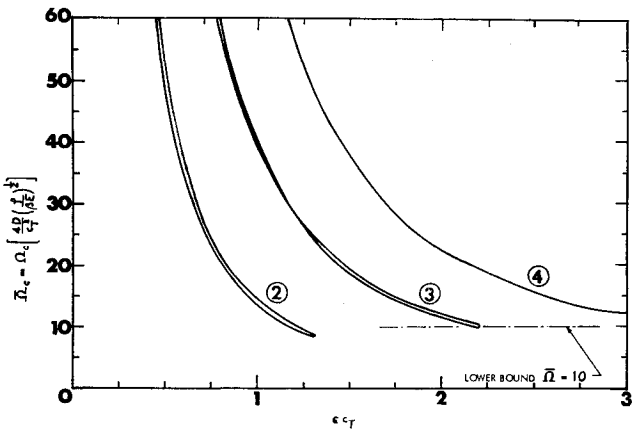

Fig. 6b) Corresponding frequency $\bar{\Omega}_c$ associated with the critical flow.

series for Y must be used to approximate adequately the shape of the body in the course of its oscillation. It was found that up to 90 terms were necessary in order to determine ω to three significant figures. The numerical computation becomes progressively more difficult when u increases above 20.0, which indicates the limit of the present computational method. It is hoped that some asymptotic analysis will be made later so that the stability conditions for large values of ϵc_T can be determined.

According to the dimensionless expressions in Eq. (11), both u and ω contain L/D, since $I = \pi D^4/64$ for a circular cross section. In order to see the effect of the slenderness ratio L/D on the stability, the ordinates of Fig. 3 are redefined as $u/(\epsilon c_T)$ and $\omega/(\epsilon c_T)^2$. A replot of Fig. 3 is shown in Fig. 6. It is seen that

$$\frac{u}{\epsilon c_T} = \frac{4}{c_T}\left(\frac{\rho}{E}\right)^{1/2} U = \bar{U}, \quad \frac{\omega}{(\epsilon c_T)^2} = \frac{4D}{c_T^2}\left(\frac{\rho}{\beta E}\right)^{1/2} \Omega = \bar{\Omega} \tag{17}$$

Thus, for a set of given parameters, the minimum critical velocity U_c remains about the same for different oscillatory modes. That is, the minimum critical velocity is independent of the slenderness ratio ϵ when ϵ is moderately large ($30 < \epsilon < 100$) as represented in Fig. 6a. The corresponding frequency Ω_c is also independent of ϵ as indicated in Fig. 6b. Therefore grossly speaking, the stability condition is mainly determined by the value of $\bar{U}$; for $\epsilon > 30$, the flow is unstable if

$$\bar{U} > 6 \tag{18}$$

while the corresponding frequency is of order

$$\bar{\Omega} = 12 \tag{19}$$

Hence, sufficient small $(E/\rho)^{1/2}$ will lead to instability. This is in qualitative agreement with results of Ortloff and Ives,[3] who showed that the cylinder motion is always unstable with zero bending rigidity EI. However, some differences between Ref. 3 and the present theory should be noted as following: 1) The moment of inertia I of the cylinder cross section is absent in Eq. (18), hence small I does not necessarily lead to instability according to the present theory, although it does according to Ref. 3. 2) In their analysis Ortloff and Ives had assumed that

$$\gamma \equiv (c_T\epsilon/4)U/\Omega L \gg 1 \tag{20}$$

based on which the complex term in the imaginary part of the complex index was neglected. However, an estimate from Eqs. (18) and (19) gives

$$\gamma \sim \frac{1}{8\beta^{1/2}} = \begin{cases} 0.177 \text{ for } \beta = 0.5 \\ 12.5 \text{ for } \beta = 10^{-4} \end{cases} \tag{21}$$

This means that the factor γ is not large compared with 1 for the case of $\beta = 0.5$ according to the present analysis. The factor γ is indeed large if $\beta \leqslant 10^{-4}$. Therefore, the analysis given by Ortloff and Ives is valid only when β is very small. In the sample calculations given by them, the values of β were kept at 10^{-3} or smaller. The reason is presumably because of the slow convergence of their solution if β is not small. Moreover, it is evident teat their solution is no longer valid for β not small. It would be interesting if one would extend their investigation to the case of $\beta = 0.5$ by relaxing the assumption of large γ in Ref. 3.

It should also be noted that for any one mode of instability, the critical velocity and frequency decrease as ϵc_T increases, which is clearly seen in Fig. 6. However, Paidoussis[1] has made an incorrect statement, based on Fig. 3, that increasing ϵc_N and ϵc_T stabilizes the system.

The eigen solutions of the system which correspond to the modal shapes of the cylinder at the marginal stability are

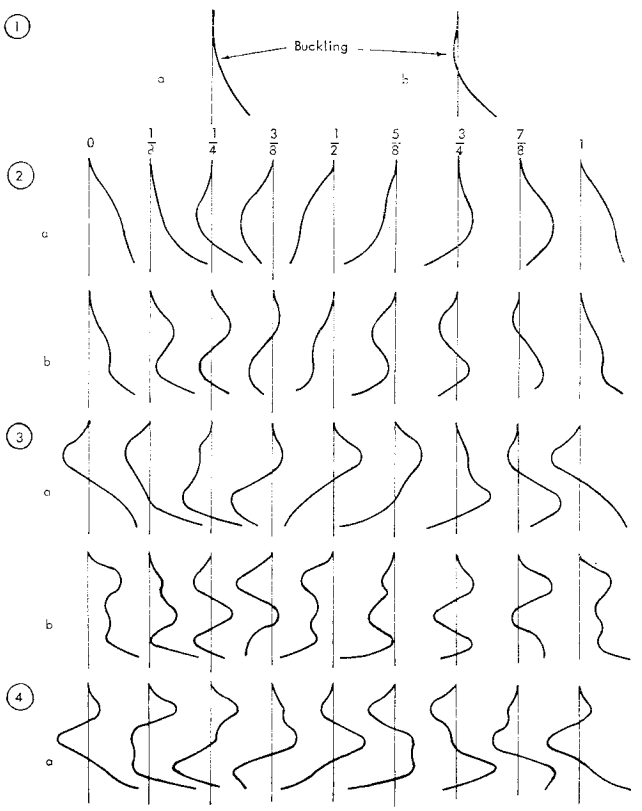

Fig. 7 Theoretical shapes of cylinders with $\epsilon c_T = \epsilon c_N = 1.0$, $\beta = 0.5$, $c'_T = 0.2$, $f = 0.7$ $\chi = 0.01$, oscillating in a condition of neutral stability; one cycle of oscillation in steps of $\frac{1}{8}\times$ period.

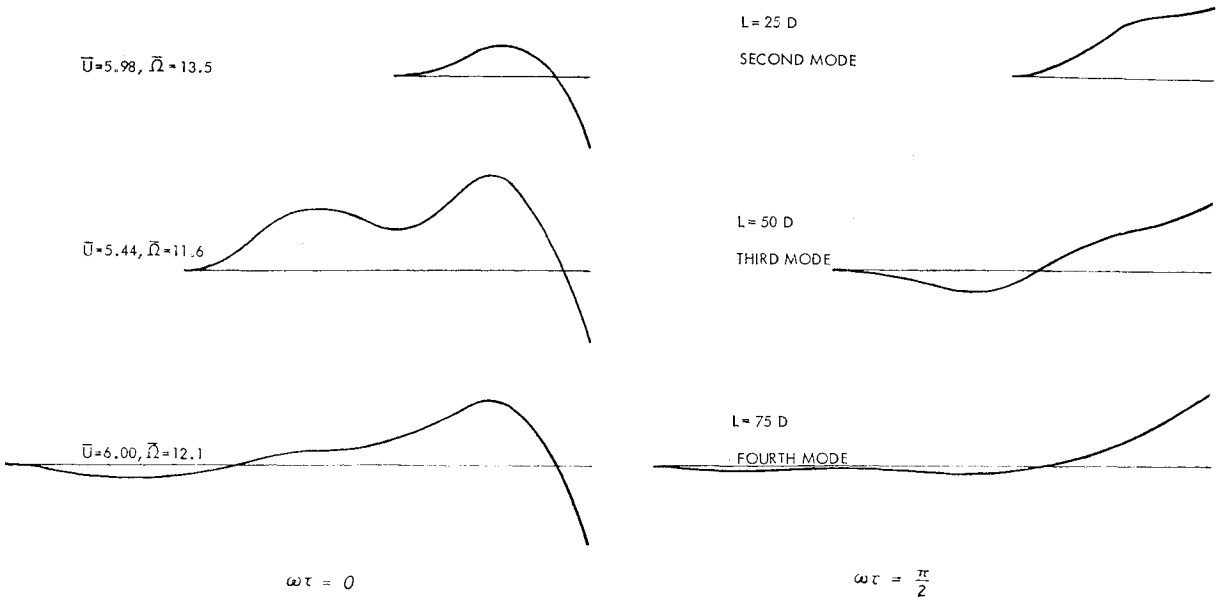

Fig. 8 Comparison of modal shapes of cylinders with L = 25D, 50D, and 75D oscillating in a condition of neutral stability ($c_T = c_N = 0.04$, $\beta = 0.5$, $c'_T = 0.2$, $f = 0.7$, $\chi = 0.01$); the figure shows the beginning and end of $\frac{1}{4}$ cycle.

shown in Fig. 7. It is seen that for given values of ϵ, χ, f, c'_T, c_T, and β, instabilities of higher modes possess larger "wave numbers," which are accompanied by higher values of u_c and ω_c. Since the mode of instability becomes higher as ϵ increases, as shown in Fig. 3, the wave number of the mode of instability also becomes larger as indicated in Fig. 8. This is also in qualitative agreement with results of Ortloff and Ives whose calculations indicated that an increase in ϵ results in instability modes of higher harmonics. A close examination of the modal shapes of the cylinder with ϵ = 25,50,75 (assuming $c_T = c_N = 0.04$), as shown in Fig. 8, reveals that for large ϵ the wave number of the instability mode, when it first sets in, is almost in proportion to ϵ. Moreover, the shapes of the cylinder near the free end portion, which is about 25 diameters in length, are almost the same for these three cases. This fact brings out an important physical mechanism of the stability of the system: the stability condition of a slender cylinder is virtually controlled by the tail portion of the cylinder which is about 25 diameters near the free end. It is seen that at ϵ = 25, 50, and 75, the instability first sets in at about the same critical velocity $\bar{U} \sim 6$ with essentially the same frequency $\bar{\Omega} \sim 12$. Although the modes of instability are all different for different values of ϵ, the behavior of the last portion of the cylinder, about 25 diameters from the tail end, is essentially the same. Physically, it is quite clear that at the last 25 diameters of the cylinders of various lengths, the kinematical and dynamical conditions are indeed very similar: free at the downstream end, clamped (or hinged) at the upstream end, with similar forces (viscous forces and the induced force required to accelerate the fluid) acting in between. It is, therefore, reasonable to expect that the critical velocities and frequencies must be about the same. The crucial question to be answered here is "why should not the system first become unstable to lower modes of instabilities before the higher modes set in?" As it has been pointed out earlier in this section, the physical reasoning is that the longitudinal tension becomes larger throughout the major portion of the cylinder as the length increases. The only exception is the tail portion near the free end, the tension of which does not change because of the increase in length. It is known, however, that an increase in tension has, in general, a stabilizing effect on the system. Consequently, the major portion of the cylinder is stabilized, because of this increase in tension. The lower modes of instabilities would have set in, had there not been an increase in tension along the cylinder. Therefore, the instability can only set in through the weakest portion of the system, namely, the tail portion where there is no increase in tension because of the increase in length. As a result, the cylinder first becomes unstable only when the tail portion starts to become unstable. With the previous mechanism in mind, it then appears quite natural that the minimum critical velocities and frequencies are virtually independent of the length of the cylinder, provided L/D is large. Therefore, caution must be exercised that $L/D \to \infty$ and $EI \to 0$ do not imply each other in this case.

4. Experiments

A number of experiments were conducted with flexible cylinders submerged and towed in a long water channel. The aim of the experiments was to test the theory discussed in the previous sections. Only some preliminary results are given here. It is hoped that subsequent paper will present more refined and extensive experimental results. The main purpose was 1) to discover whether the various types of instability predicted by theory do in fact occur, 2) to supplement Paidoussis' experiments[2] by using a towing system in otherwise stationary fluid, and 3) to provide some experimental data, particularly regarding the thresholds of the various instabilities and the drag coefficient, for quantitative comparison with theory.

4.1 Apparatus

The apparatus consisted of an 85-ft towing tank. The cylinder was glued to a horizontal metal boom which was rigidly connected to a vertical aerofoil strut, as shown in Fig. 9. Rubber tubes were used for the flexible cylinders in the experiment. Two kinds of cylinders were used: cylinder I was 0.312-in. outer diam and 0.187-in. inner diam (EI = 0.2140 lb-in.^{2}), and cylinder II was 0.230-in. outer diam and 0.110-in. inner diam (EI = 0.0345 lb-in.^{2}). Cylinder I, being heavier than water, was made almost neutral buoyant by sealing the ends and leaving the inside hollow. Cylinder II, being lighter than water, was made neutral buoyant by filling the inside with glycerin and then sealing the ends. Various lengths were used from several inches to a few feet. The free end of the rubber tube was blunt and no tapered end pieces were used. The maximum towing speed attainable was about 13 fps. In each towing, the speed was set at a fixed value. The speed was recorded in short-time intervals during each

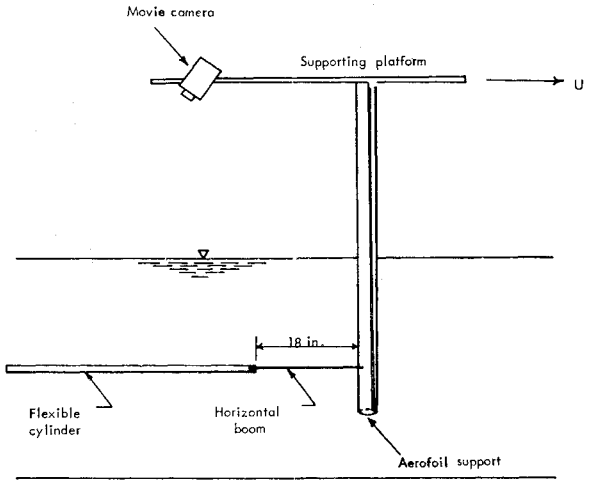

Fig. 9 Schematic diagram of the apparatus used for experiments.

towing. It was found that the towing speed was constant throughout the major portion of the towing tank. Hence, the assumption of steady and uniform flow in the theory is satisfied.

4.2 General Observations

In each test, the towing speed was increased in small steps, starting from zero. In some of the early experiments, the vertical support was not in an aerofoil shape and no horizontal metal boom was used. It was found that the instabilities occurred at much lower flow velocities than that predicted by the theory. This is probably because of the wake produced by the vertical strut. The instability of the wake has definitely a strong influence on the instability of the cylinder. For most experiments, however, the vertical strut was made in an aerofoil shape and a horizontal metal boom was used so that fluctuations in the wake became much weaker in the vicinity of the cylinder.

With the present system, the buckling is somewhat difficult to detect. However, the oscillatory modes were fairly easy to observe. Thus in these preliminary experiments, only the thresholds of instability and associated frequency for the oscillatory mode were recorded. The frequencies are in general quite low, in the range of 1–3 cps. They were recorded with the help of a stop watch. The shape of the cylinder, when oscillation set in, was in general agreement with the theory that the amplitude of the oscillation is relatively large near the tail. It is found that the critical velocity and frequency remain essentially the same as L/D increases beyond 100.

4.3 Quantitative Comparison with Theory

Direct quantitative comparison depends heavily on the accuracy of the drag coefficients c_T and c_N which is evident in Fig. 3. Therefore, some measurements of the drag force on the cylinders at various speeds were made. *LVDT* force block was used to obtain the drag force on the submerged system. The drag force on the cylinder was obtained by two separate runs at the same speed—one with cylinder and the other without. The difference in the forces measured gave the drag force on the cylinder. This, of course, included both the friction and form drag. The form drag is, however, very small compared with the friction drag for large L/D. The experimental data for drag measurements were summarized in Table 1. It is seen that c_T is in the range 0.04–0.07.

For purposes of comparison, experimental values of thresholds of instability were compared with theory. The critical velocities and frequencies for $c_N = c_T = 0.04$ and 0.06 are compared with theoretical values in Fig. 3. The agreement is reasonably good.

Table 1 Measurement of drag coefficient

Run No.	Towing speed, cm/sec	Length, cm	ϵ	Drag, 10^3 dyne	c_T
1	177	14.6	25	15.0	0.0493
2	94.8	29.2	50	13.5	0.0785
3	178	58.3	100	51.0	0.0508
4	237	58.3	100	101.	0.0470
5	94.8	175.0	300	70.4	0.0683
6	130	175.0	300	94.6	0.0487
7	178	175.0	300	242.	0.0665
8	237	175.0	300	291.	0.0453
				Average	0.0568

5. Conclusions

The experiments, conducted with apparatus of the simplest kind, appeared to confirm the essential features of the dynamical problem as predicted by theory. A few important conclusions can be summarized below: 1) The stability of a towed slender cylinder is virtually controlled by the tail portion of the cylinder which is about 25 diameters from the free end. 2) For fixed value of L/D, higher modes of oscillation set in as the velocity U increases. 3) For a certain critical mode, the critical velocity and frequency decrease as L/D increases. 4) As L/D increases, the minimum critical speed, frequency, and effective wave length, that mark the threshold of instability, virtually remain at the same magnitude. 5) The lower modes of instabilities are filtered out and only the higher modes of instabilities set in as L/D increases. 6) For $L/D > 30$, the critical velocity is $U_c[(4/c_T)(\rho/E)^{1/2}] \sim 6$ and the associated frequency is $\Omega_c[(4D/c_T^2)(\rho/\beta E)^{1/2}] \sim 12$.

It is planned that future work will include 1) an asymptotic analysis for $\epsilon \to \infty$, 2) more experimental investigation, 3) the effect of initial curvature, and 4) forcing effect because of the wake of the vertical strut.

References

[1] Paidoussis, M. P., "Dynamics of Flexible Slender Cylinders in Axial Flow; Part 1. Theory," *Journal of Fluid Mechanics*, Vol. 26, 1966, pp. 717–736.

[2] Paidoussis, M. P., "Dynamics of Flexible Slender Cylinders in Axial Flow; Part 2. Experiment," *Journal of Fluid Mechanics*, Vol. 26, 1966, pp. 737–751.

[3] Ortloff, C. R. and Ives, J. "On the Dynamic Motion of a Thin Flexible Cylinder in a Viscous Stream," *Journal of Fluid Mechanics*, Vol. 38, 1969, pp. 713–720.

[4] Gregory, R. W. and Paidoussis, M. P., "Unstable Oscillation of Tubular Cantilevers Conveying Fluid; I. Theory," *Proceedings of the Royal Society*, Vol. A293, 1966, pp. 512–527.

[5] Reber, R. K., "The Configuration and Towing Tension of Towed Sweep Cables Supported by Floats," Rept. 75, Feb. 1944, Bureau of Ships.

[6] Hoerner, S. F., *Aerodynamic Drag*, published by author, 1951.

[7] Hoerner, S. F., *Fluid Dynamic Drag*, published by author, 1958.

[8] Taylor, G. I., "Analysis of the Swimming of Long and Narrow Animals," *Proceedings of the Royal Society*, Vol. A214, pp. 158–183.

[9] Parsons, M. G. and Casarella, M. J., "A Survey of Studies on the Configuration of Cable Systems under Hydrodynamic Loading," TR 69-1, May 1959, Dept. of Mechanical Engineering, The Catholic University of America, Washington, D.C.

[10] Munk, M. M., "The Aerodynamic Forces on Airship Hulls," Rept. 184, 1923, NACA, pp. 451–468.

[11] Hawthorne, W. R., "The Early Development of the Dracone Flexible Barge," *Proceedings of Institution of Mechanical Engineerings*, Vol. 175, pp. 52–83.